Editors' Suggestion

Efficient Experimental Verification of Quantum Gates with Local Operations

Rui-Qi Zhang,[1,2,*] Zhibo Hou,[1,2,*] Jun-Feng Tang,[1,2] Jiangwei Shang,[3,†] Huangjun Zhu,[4,5,6,‡] Guo-Yong Xiang,[1,2,§] Chuan-Feng Li,[1,2] and Guang-Can Guo[1,2]

[1]*CAS Key Laboratory of Quantum Information, University of Science and Technology of China, Hefei 230026, People's Republic of China*

[2]*CAS Center For Excellence in Quantum Information and Quantum Physics, University of Science and Technology of China, Hefei 230026, People's Republic of China*

[3]*Key Laboratory of Advanced Optoelectronic Quantum Architecture and Measurement of Ministry of Education, School of Physics, Beijing Institute of Technology, Beijing 100081, China*

[4]*State Key Laboratory of Surface Physics and Department of Physics, Fudan University, Shanghai 200433, China*

[5]*Institute for Nanoelectronic Devices and Quantum Computing, Fudan University, Shanghai 200433, China*

[6]*Center for Field Theory and Particle Physics, Fudan University, Shanghai 200433, China*

(Received 27 June 2021; accepted 24 November 2021; published 14 January 2022)

Verifying the correct functioning of quantum gates is a crucial step toward reliable quantum information processing, but it becomes an overwhelming challenge as the system size grows due to the dimensionality curse. Recent theoretical breakthroughs show that it is possible to verify various important quantum gates with the optimal sample complexity of $O(1/\epsilon)$ using local operations only, where ϵ is the estimation precision. In this Letter, we propose a variant of quantum gate verification (QGV) that is robust to practical gate imperfections and experimentally realize efficient QGV on a 2-qubit controlled-not gate and a 3-qubit Toffoli gate using only local state preparations and measurements. The experimental results show that, by using only 1600 and 2600 measurements on average, we can verify with 95% confidence level that the implemented controlled-not gate and Toffoli gate have fidelities of at least 99% and 97%, respectively. Demonstrating the superior low sample complexity and experimental feasibility of QGV, our work promises a solution to the dimensionality curse in verifying large quantum devices in the quantum era.

DOI: 10.1103/PhysRevLett.128.020502

Introduction.—Quantum computers can perform computational tasks much more efficiently [1,2] and even exponentially faster than their classical counterparts [3–5]. Before harnessing the power of a quantum computer, a crucial step is to verify the correct functioning of its building blocks, i.e., the quantum gates. Traditional quantum process tomography (QPT) [6,7] can provide the complete information of a quantum gate and is a feasible solution for small systems. However, QPT is not scalable, as its complexity grows exponentially with the size of the quantum system, and so far has been applied to quantum gates acting on no more than three qubits [8–10]. This exponential resource cost cannot be circumvented in general, even if one can take advantage of the sparsity of the underlying structures [11–13] or heuristic algorithms [14,15].

The key observation toward efficient verification of a quantum gate is that the complete information of a quantum gate is usually not necessary in many tasks. Quite often, the fidelity of a quantum gate is enough to characterize its quality. Fidelity estimation based on unitary 2-designs and the twirling protocol [16,17] can estimate the fidelity of a Clifford gate with size-independent sample complexity of $O(1/\epsilon^2)$, where ϵ is the estimation precision. Direct fidelity estimation and Monte Carlo sampling [18–20] can achieve a similar sample complexity for Clifford and other well-conditioned gates even if one can only prepare product states and perform Pauli measurements. Randomized benchmarking (RB) [21–24] can certify Clifford gates and some special non-Clifford gates with a similar sample complexity and possesses the additional advantage of robustness against state-preparation and measurement errors.

Despite the progress mentioned above, most approaches in the literature have disadvantages, which limit their applicability. Notably, most approaches are limited to a few types of quantum gates (say, Clifford gates) [16–21]. In addition, they have a suboptimal scaling behavior in the precision ϵ. Moreover, many approaches, including twirling protocols and RB, require entangling operations [16,17,21–24], that is, preparing entangled states or performing entangling measurements.

Recently, an alternative approach called quantum gate verification (QGV) or quantum process verification [25–27] has been developed to tackle these problems. It is inspired by probabilistic verification protocols that have found fruitful applications in certifying quantum states [28–32] and entanglement [33,34]. With this approach, a variety of quantum gates can be verified efficiently with the optimal sample complexity of $O(1/\epsilon)$ using only local state preparations and

measurements. Nevertheless, the current formulation of QGV can reach a valid conclusion only when the gate to be verified passes all the tests, which may prevent QGV from obtaining a valid conclusion when a realistic quantum gate with acceptable infidelity is considered.

In this Letter, we propose a variant of QGV that is tolerant to gate imperfections, while keeping its efficiency. With this robust proposal, we experimentally apply QGV to a 2-qubit controlled-not (CNOT) gate realized in a photonic system. By using 20 experimental settings and 1600 samples on average, we can verify that the CNOT gate has at least 99% fidelity with a 95% confidence level. We then apply QGV to a 3-qubit Toffoli gate to illustrate the scalability and superiority of QGV. By using 32 measurement settings and 2600 samples on average, we can verify that the fidelity of the Toffoli gate is at least 97% with a 95% confidence level. By contrast, the standard QPT would require at least 4096 measurement settings and over a million measurements in total to characterize the Toffoli gate. Our experiments demonstrate that efficient verification of quantum gates can be achieved with only local state preparations and measurements.

Theoretical framework.—Consider a quantum device that is expected to implement a target unitary transformation $\mathcal{U}$, but actually realizes N unknown quantum channels $\Lambda_1, \ldots, \Lambda_N$, which are assumed to be identical and independent, over the N runs. In practice, these channels might deviate from $\mathcal{U}$. Let $1-\epsilon_A$ be the average gate fidelity of the channels with respect to $\mathcal{U}$. Our goal is to verify, with some confidence level $1-\delta$ (significance level δ), that the average gate infidelity of the channels is not larger than a given threshold ϵ, i.e.,

$$\epsilon_A \le \epsilon, \quad \text{with confidence level } 1-\delta. \tag{1}$$

The verification procedure, illustrated in Fig. 1, can be described as follows [26]. In the ith run, the verifier first randomly chooses a pure state $\rho_j = |\psi_j\rangle\langle\psi_j|$ with probability p_j from a set of test states $\{\rho_j\}_j$ and subjects it to the device. Then the verifier performs a two-outcome measurement $\{M_l^{(j)}, \mathbb{1} - M_l^{(j)}\}$, which is called a test, on the output state $\Lambda_i(\rho_j)$ with outcome 1 for passing and 0 for failure. Here the test operator $M_l^{(j)}$ needs to satisfy the condition $\mathrm{Tr}[M_l^{(j)}\mathcal{U}(\rho_j)] = 1$ and is chosen randomly with the conditional probability $p_{l|j}$ from a test set $\{M_l^{(j)}\}_l$ that depends on $\mathcal{U}(\rho_j)$. The verifier records the test results of the N runs and compares the passing rate $\hat{p}_s$ with a given threshold p_A, based on which the device is accepted or rejected.

The performance of the above verification procedure is mainly determined by the "process verification operator" defined as [26]

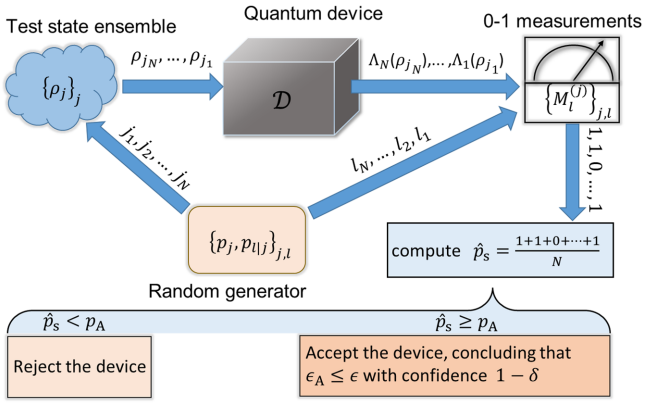

FIG. 1. Procedure for verifying the quantum device $\mathcal{D}$. In each run, the random number generator generates random numbers j and l according to the probabilities p_j and $p_{l|j}$ (conditioned on j), respectively. Then state ρ_j is drawn from the set of test states and sent to $\mathcal{D}$; next, the measurement module implements a two-outcome measurement $\{M_l^{(j)}, \mathbb{1} - M_l^{(j)}\}$ on the output state $\Lambda(\rho_j)$. By repeating the above procedure N times, the verifier can reach a conclusion on the quality of $\mathcal{D}$ based on the passing rate $\hat{p}_s$ over the N tests.

$$\Theta := d\sum_j p_j \mathcal{U}^{-1}\left(\sum_l p_{l|j} M_l^{(j)}\right) \otimes \rho_j^*. \tag{2}$$

For a perfect device, the passing probability p_s is unity. If the quantum gate realized has (average gate) infidelity ϵ, by contrast, the acceptance probability is upper bounded by $[p_A(\Theta, \epsilon)]^N$, where $p_A(\Theta, \epsilon)$ is defined as the maximal passing probability for quantum gates with infidelity $\epsilon_A \ge \epsilon$ given the verification operator Θ [26]. If we set $p_A = 1$, then the minimal number of tests required to verify the quantum gate with infidelity ϵ and confidence level $1-\delta$ reads

$$N(\epsilon, \delta, \Theta) = \left\lceil \frac{\ln \delta}{\ln p_A(\Theta, \epsilon)} \right\rceil. \tag{3}$$

This number is minimized when the test states ρ_j form a 2-design [35,36] and the test operator for each test state ρ_j is chosen to be the projector $\mathcal{U}(\rho_j)$ onto the target output state, in which case $p_A(\Theta, \epsilon) = 1 - \epsilon$, and Eq. (3) reduces to [26]

$$N^{\mathrm{opt}}(\epsilon, \delta) = \left\lceil \frac{\ln \delta}{\ln(1-\epsilon)} \right\rceil \overset{\epsilon \to 0}{\approx} \frac{\ln \delta^{-1}}{\epsilon}. \tag{4}$$

In general, to realize the optimal verification protocol mentioned above would require entangling operations, which are often inaccessible. Fortunately, for many important quantum gates, nearly optimal performance can be achieved using local state preparations and local projective measurements only [25–27]. For simplicity, in this Letter we focus on verification protocols that are balanced, which means the set of test states satisfies the condition

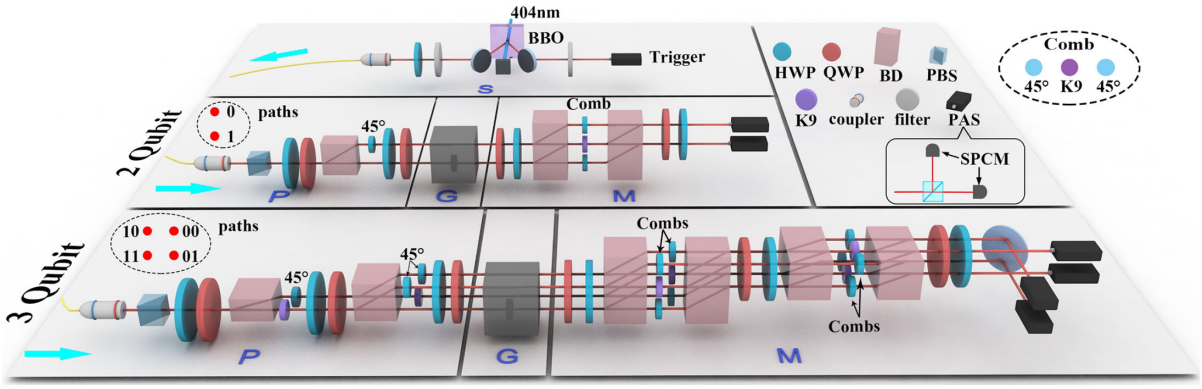

FIG. 2. Experimental setup. The heralded single-photon source (labeled by S) is realized by spontaneous parametric down-conversion in a type-I BBO crystal. The figure shows two independent setups employed for implementing the verification protocols for the 2-qubit CNOT gate and 3-qubit Toffoli gate, respectively. Each setup consists of three modules: a state-preparation module (labeled by P), a quantum gate module (labeled by G), and a measurement module (labeled by M). The inset in the component panel (upper right) shows the details of the polarization analyzing system (PAS). Each PAS consists of one polarizing beam splitter (PBS) and two single-photon counting modules (SPCMs) and can measure the photons in the $\{|H\rangle, |V\rangle\}$ polarization basis. BD, beam displacer; K9, K9 glass plate with the same optical length as other wave plates used.

$\sum_j p_j \rho_j = \mathbb{1}/d$, where d is the dimension of the underlying Hilbert space. Denote by $\nu := \nu(\Theta)$ the spectral gap of Θ (between the largest and the second largest eigenvalues), then we have

$$N^{\text{local}}(\epsilon, \delta, \Theta) \leq \left\lceil \frac{\ln \delta}{\ln(1-\nu\epsilon)} \right\rceil \leq \left\lceil \frac{\ln \delta^{-1}}{\nu\epsilon} \right\rceil. \tag{5}$$

In practice, quantum gates are never perfect. Even if they satisfy the condition $\epsilon_A \leq \epsilon$, a few failure events might happen with a non-negligible probability among the N tests. In this case, setting $p_A = 1$ for the threshold would reject a properly functioning device with certain probability. To remedy this problem and construct a robust verification protocol, we need to consider the situation with $0 < \epsilon_A \leq \epsilon$. To be concrete, if the passing rate $\hat{p}_s$ over the N tests is larger than $p_A(\Theta, \epsilon)$, then the significance level $\delta(\hat{p}_s)$ that the device satisfies $\epsilon_A \leq \epsilon$ is upper bounded by

$$\delta(\hat{p}_s) \leq e^{-D(\hat{p}_s \| p_A(\Theta,\epsilon))N}, \tag{6}$$

where $D(x\|y) = x\ln(x/y) + (1-x)\ln[(1-x)/(1-y)]$ is the Kullback-Leibler divergence. On the other hand, given a significance level δ, we can derive from Eq. (6) an upper bound for the infidelity ϵ_A, that is,

$$\epsilon_A \leq \frac{d}{d+1} \frac{1 - D^{(-1)}(\hat{p}_s, (\ln \delta^{-1})/N)}{\nu(\Theta)}, \tag{7}$$

where $D^{(-1)}(\hat{p}_s, y)$ is the inverse function of $y = D(\hat{p}_s\|x)$ with domain $0 \leq x < \hat{p}_s$ (for a fixed $\hat{p}_s$). The detailed derivations of Eqs. (6) and (7) are relegated to Sec. S1 in the Supplemental Material [37].

Experimental setup.—The experimental setups for verifying 2- and 3-qubit quantum gates are shown in Fig. 2. Both of them consist of three modules: a state-preparation module, a quantum gate module, and a measurement module. Here we use the path and polarization degrees of freedom (d.o.f.) of the heralded photon to encode the test state employed in the verification protocol. The 2-qubit system consists of a path d.o.f. with up and down modes and a polarization d.o.f. with horizontal (H) and vertical (V) polarizations; by contrast, the 3-qubit system consists of a path d.o.f. with left-right modes and up-down modes and a polarization d.o.f.

The heralded single-photon source shown in Fig. 2 is used by both setups. An ultraviolet laser with central wavelength of 404 nm is used to pump a type-I phase-matched β-barium-borate (BBO) crystal to generate a photon pair in the product (polarization) state via spontaneous parametric down-conversion [40]. One photon is measured as a trigger to herald the generation of its twin photon, which is then transmitted to the state-preparation module.

The state-preparation module in the 2-qubit (3-qubit) setup is designed to prepare arbitrary 2-qubit (3-qubit) product states by virtue of photonic quantum walks. Here the coin operators required are realized by combinations of half-wave plates (HWPs) and quarter-wave plates (QWPs), as described in Sec. S2 of the Supplemental Material [37]. The K9 plates are pieces of glass and are used to compensate for the path-length differences among the interference arms in the state-preparation module in the 3-qubit setup.

The quantum gate module implements the quantum gate to be verified, which can be seen as a black box that is

expected to perform the target unitary transformation on the input quantum states. The measurement module in the 2-qubit (3-qubit) setup is designed to realize arbitrary local projective measurements on 2-qubit (3-qubit) systems by using photonic quantum walks. The QWP-HWP pairs inside the measurement module control the measurement settings for individual qubits; see Sec. S2 of the Supplemental Material [37]. In addition, the K9 plates are used to compensate for the path-length differences among the interference arms. Finally, the heralded photon is collected by two PASs in the 2-qubit setup and four PASs in the 3-qubit setup, where the PASs measure the polarization of the input photon in the $\{|H\rangle, |V\rangle\}$ basis.

Results.—To demonstrate the efficiency and scalability of QGV, we performed QGV on a 2-qubit CNOT gate and a 3-qubit Toffoli gate. The CNOT gate (Toffoli gate) is implemented by inserting a HWP with its optical axis aligned at 45° from the horizontal direction on path 1 (11) in the 2-qubit (3-qubit) setup. The sets of test states and measurement settings employed for verifying the CNOT gate and Toffoli gate are detailed in Sec. S3 of the Supplemental Material [37].

The performance of QGV is characterized by the scalings of the significance level δ and infidelity ϵ_A with respect to the number of tests N. Here we only offer an upper bound for δ (ϵ_A) when ϵ_A (δ) is fixed. After each test, the bounds for δ and ϵ_A are determined from the test results by virtue of Eqs. (6) and (7). Since the results of a single run of QGV suffer from statistical fluctuations, which would prevent us from reliably evaluating the performance, we repeat the verification procedure 50 times under the same conditions (e.g., the set of test states and the number of tests in total). The average values of δ and ϵ_A are calculated by replacing $\hat{p}_s$ in Eqs. (6) and (7) with $\sum_{i=1}^{50} \hat{p}_s^{(i)}/50$ for each value of N, where $\hat{p}_s^{(i)}$ is the passing rate of the ith run among the first N tests. We also use Eqs. (6) and (7) to fit the average results by fixing the value of $\hat{p}_s$ to be the average passing rate over the 50 runs of QGV among all the tests used.

The experimental results on the verification of the CNOT gate are shown in Fig. 3, where 20 different measurement settings and 6000 tests in total (see Sec. S3 of the Supplemental Material [37] for details) are used in each run of QGV. In Fig. 3(a), where ϵ is set to be 0.01, δ rapidly drops below 0.05 within 1600 tests for both the single-run and average results, which means that the CNOT gate is verified efficiently with high confidence level. Alternatively, we can set the confidence level $1-\delta$ to be 0.95 and calculate ϵ_A. Figure 3(b) shows that ϵ_A descends below 0.01 after 1600 tests for both the single-run and average results, which is consistent with Fig. 3(a). The scaling of the average infidelity ϵ_A with respect to N can be described by the power law $N^{-0.857}$ within the first 200 tests, which is quite close to the optimal scaling of N^{-1} in Eq. (4). After 200 tests, the descending speed of ϵ_A gradually slows down as it gets closer to the actual infidelity and eventually converges to

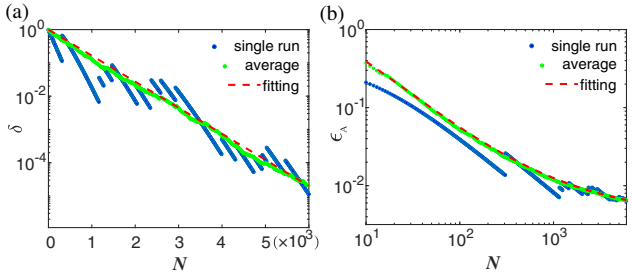

FIG. 3. Experimental results on the verification of the CNOT gate. The blue dots represent the results of a single run of QGV. The green dots represent the average results of 50 runs of QGV. The red dotted line is the fitting line for the average results. (a) When ϵ is set to 0.01, δ is log plotted versus N. (b) When δ is set to 0.05, ϵ_A is log-log plotted versus N. Within the first 200 tests, the scaling of ϵ_A averaged over 50 runs with respect to N is fitted to be $N^{-0.857}$ by linear regression. The error bars of ϵ_A are detailed in Sec. S6 of the Supplemental Material [37].

0.0040 after 10 000 tests (see Sec. S4 of the Supplemental Material [37]). The estimation error of ϵ_A versus N is shown in Sec. 6 of the Supplemental Material [37]. The effects of systematic errors are analyzed in Sec. 7 of the Supplemental Material [37]. In both plots in Fig. 3, the single-run results break up into discrete short segments due to the occasional failures caused by the deviation of the actual CNOT gate from the ideal target gate.

We then perform QPT on the CNOT gate and find that the actual average gate fidelity is 99.7% with standard deviation of 0.004%, which is consistent with the QGV result. To perform QPT on the CNOT gate, we employ 36 product Pauli eigenstates as the test states and nine measurement settings based on Pauli measurements for each output state. The experimental details are relegated to Sec. S5 of the Supplemental Material [37]. Here the total number of experimental settings is 324, and the total number of measurements is over 6×10^6, which is substantially more than that required in QGV (the number of measurements in QPT can be reduced, but the conclusion does not change, as explained in Sec. S8 of the Supplemental Material [37]). These facts clearly reflect the advantage of QGV over QPT.

To demonstrate the scalability of QGV, next we consider the verification of the 3-qubit Toffoli gate. In this case, 32 different experimental settings and 10 000 tests in total are employed in each run of QGV (see Sec. S3 of the Supplemental Material [37] for details). The verification results are shown in Fig. 4, which are analogous to the counterparts shown in Fig. 3. To verify the Toffoli gate within infidelity 0.03 and confidence level 95%, only 2600 tests are required. In Fig. 4(b), ϵ_A exhibits $N^{-0.840}$ scaling with respect to N within the first 200 tests, which is also close to the optimal scaling of N^{-1}. The infidelity estimator ϵ_A eventually converges to 0.0148 after 40 000 tests; see Sec. S4 of the Supplemental Material [37]. The estimation error of ϵ_A for the Toffoli gate versus N is shown in Sec. S6

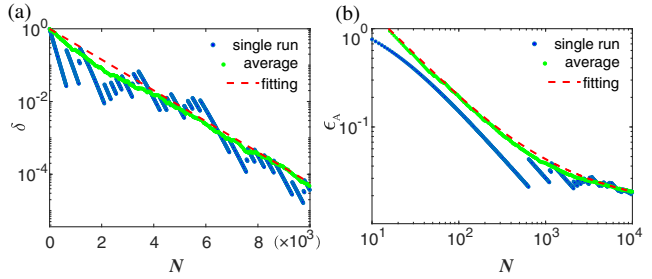

FIG. 4. Experimental results on the verification of the Toffoli gate. The meanings of the data points are similar to those in Fig. 3. (a) When ϵ is set to 0.03, δ is log plotted versus N. (b) When δ is set to 0.05, ϵ_A is log-log plotted versus N. Within the first 200 tests, the scaling of ϵ_A averaged over 50 runs with respect to N is fitted to be $N^{-0.840}$ by linear regression. The error bars of ϵ_A are detailed in Sec. S6 of the Supplemental Material [37].

of the Supplemental Material [37]. In both plots in Fig. 4, the single-run results break up more frequently than their counterparts in Fig. 3, due to the larger deviation of the actual Toffoli gate from the ideal Toffoli gate. Incidentally, to perform QPT on the Toffoli gate would require $8^4 = 4096$ experimental settings and millions of measurements in total, which are quite prohibitive and much more resource consuming than QGV.

Summary.—By virtue of photonic systems, we experimentally realized efficient verification of a CNOT gate and a Toffoli gate with local state preparations and measurements. The experimental results clearly show that the verification protocols can achieve nearly optimal performance without relying on entangling operations and are substantially more efficient than QPT. Moreover, they are scalable and robust to the imperfections of the actual quantum gates. Notably, only 2600 tests are required to verify the Toffoli gate with fidelity 97% and confidence level 95%. Our work demonstrates that QGV is a powerful tool for verifying quantum gates and quantum devices, and may play a key role in the development of quantum technologies.

The work at the University of Science and Technology of China is supported by the National Key Research and Development Program of China (Grant No. 2018YFA0306400), the National Natural Science Foundation of China (Grants No. 61905234, No. 11974335, No. 11574291, No. 11774334, and No. 12134014), the Key Research Program of Frontier Sciences, CAS (Grant No. QYZDYSSW-SLH003), USTC Research Funds of the Double First-Class Initiative (Grant No. YD2030002007), and the Fundamental Research Funds for the Central Universities (Grant No. WK2470000035). J. S. acknowledges support by the National Natural Science Foundation of China (Grants No. 12175014 and No. 11805010). The work at Fudan University is supported by the National Natural Science Foundation of China (Grants No. 92165109 and No. 11875110) and Shanghai Municipal Science and Technology Major Project (Grant No. 2019SHZDZX01).

*R.-Q. Z. and Z. H. contributed equally to this work.
†jiangwei.shang@bit.edu.cn
‡zhuhuangjun@fudan.edu.cn
§gyxiang@ustc.edu.cn

[1] A. W. Harrow, A. Hassidim, and S. Lloyd, Quantum Algorithm for Linear Systems of Equations, Phys. Rev. Lett. **103**, 150502 (2009).
[2] L. K. Grover, A fast quantum mechanical algorithm for database search, in *Proceedings of the Twenty-Eighth Annual ACM Symposium on Theory of Computing*, STOC '96 (Association for Computing Machinery, New York, NY, USA, 1996), pp. 212–219.
[3] P. Shor, Algorithms for quantum computation: Discrete logarithms and factoring, in *Proceedings of the 35th Annual Symposium on Foundations of Computer Science* (Institute of Electrical and Electronics Engineers, Santa Fe, 1994), pp. 124–134.
[4] S. Aaronson and A. Arkhipov, The computational complexity of linear optics, in *Proceedings of the Forty-Third Annual ACM Symposium on Theory of Computing*, STOC '11 (Association for Computing Machinery, New York, NY, USA, 2011), pp. 333–342.
[5] H.-S. Zhong *et al.*, Quantum computational advantage using photons, Science **370**, 1460 (2020).
[6] I. L. Chuang and M. A. Nielsen, Prescription for experimental determination of the dynamics of a quantum black box, J. Mod. Opt. **44**, 2455 (1997).
[7] J. F. Poyatos, J. I. Cirac, and P. Zoller, Complete Characterization of a Quantum Process: The Two-Bit Quantum Gate, Phys. Rev. Lett. **78**, 390 (1997).
[8] M. Riebe, K. Kim, P. Schindler, T. Monz, P. O. Schmidt, T. K. Körber, W. Hänsel, H. Häffner, C. F. Roos, and R. Blatt, Process Tomography of Ion Trap Quantum Gates, Phys. Rev. Lett. **97**, 220407 (2006).
[9] R. C. Bialczak, M. Ansmann, M. Hofheinz, E. Lucero, M. Neeley, A. D. O'Connell, D. Sank, H. Wang, J. Wenner, M. Steffen, A. N. Cleland, and J. M. Martinis, Quantum process tomography of a universal entangling gate implemented with Josephson phase qubits, Nat. Phys. **6**, 409 (2010).
[10] Y. S. Weinstein, T. F. Havel, J. Emerson, N. Boulant, M. Saraceno, S. Lloyd, and D. G. Cory, Quantum process tomography of the quantum Fourier transform, J. Chem. Phys. **121**, 6117 (2004).
[11] D. Gross, Y.-K. Liu, S. T. Flammia, S. Becker, and J. Eisert, Quantum State Tomography via Compressed Sensing, Phys. Rev. Lett. **105**, 150401 (2010).
[12] S. T. Flammia, D. Gross, Y.-K. Liu, and J. Eisert, Quantum tomography via compressed sensing: Error bounds, sample complexity and efficient estimators, New J. Phys. **14**, 095022 (2012).
[13] M. Cramer, M. B. Plenio, S. T. Flammia, R. Somma, D. Gross, S. D. Bartlett, O. Landon-Cardinal, D. Poulin, and Y.-K. Liu, Efficient quantum state tomography, Nat. Commun. **1**, 149 (2010).

[14] C. Ferrie, Self-Guided Quantum Tomography, Phys. Rev. Lett. **113**, 190404 (2014).
[15] Z. Hou, J.-F. Tang, C. Ferrie, G.-Y. Xiang, C.-F. Li, and G.-C. Guo, Experimental realization of self-guided quantum process tomography, Phys. Rev. A **101**, 022317 (2020).
[16] C. Dankert, R. Cleve, J. Emerson, and E. Livine, Exact and approximate unitary 2-designs and their application to fidelity estimation, Phys. Rev. A **80**, 012304 (2009).
[17] D. Lu, H. Li, D.-A. Trottier, J. Li, A. Brodutch, A. P. Krismanich, A. Ghavami, G. I. Dmitrienko, G. Long, J. Baugh, and R. Laflamme, Experimental Estimation of Average Fidelity of a Clifford Gate on a 7-Qubit Quantum Processor, Phys. Rev. Lett. **114**, 140505 (2015).
[18] S. T. Flammia and Y.-K. Liu, Direct Fidelity Estimation from Few Pauli Measurements, Phys. Rev. Lett. **106**, 230501 (2011).
[19] M. P. da Silva, O. Landon-Cardinal, and D. Poulin, Practical Characterization of Quantum Devices without Tomography, Phys. Rev. Lett. **107**, 210404 (2011).
[20] L. Steffen, M. P. da Silva, A. Fedorov, M. Baur, and A. Wallraff, Experimental Monte Carlo Quantum Process Certification, Phys. Rev. Lett. **108**, 260506 (2012).
[21] E. Magesan, J. M. Gambetta, B. R. Johnson, C. A. Ryan, J. M. Chow, S. T. Merkel, M. P. da Silva, G. A. Keefe, M. B. Rothwell, T. A. Ohki, M. B. Ketchen, and M. Steffen, Efficient Measurement of Quantum Gate Error by Interleaved Randomized Benchmarking, Phys. Rev. Lett. **109**, 080505 (2012).
[22] R. Harper and S. T. Flammia, Estimating the fidelity of T gates using standard interleaved randomized benchmarking, Quantum Sci. Technol. **2**, 015008 (2017).
[23] E. Onorati, A. H. Werner, and J. Eisert, Randomized Benchmarking for Individual Quantum Gates, Phys. Rev. Lett. **123**, 060501 (2019).
[24] S. Garion, N. Kanazawa, H. Landa, D. C. McKay, S. Sheldon, A. W. Cross, and C. J. Wood, Experimental implementation of non-Clifford interleaved randomized benchmarking with a controlled-S gate, Phys. Rev. Research **3**, 013204 (2021).
[25] Y.-C. Liu, J. Shang, X.-D. Yu, and X. Zhang, Efficient verification of quantum processes, Phys. Rev. A **101**, 042315 (2020).
[26] H. Zhu and H. Zhang, Efficient verification of quantum gates with local operations, Phys. Rev. A **101**, 042316 (2020).
[27] P. Zeng, Y. Zhou, and Z. Liu, Quantum gate verification and its application in property testing, Phys. Rev. Research **2**, 023306 (2020).
[28] M. Hayashi, K. Matsumoto, and Y. Tsuda, A study of LOCC-detection of a maximally entangled state using hypothesis testing, J. Phys. A **39**, 14427 (2006).
[29] S. Pallister, N. Linden, and A. Montanaro, Optimal Verification of Entangled States with Local Measurements, Phys. Rev. Lett. **120**, 170502 (2018).
[30] W.-H. Zhang, C. Zhang, Z. Chen, X.-X. Peng, X.-Y. Xu, P. Yin, S. Yu, X.-J. Ye, Y.-J. Han, J.-S. Xu, G. Chen, C.-F. Li, and G.-C. Guo, Experimental Optimal Verification of Entangled States using Local Measurements, Phys. Rev. Lett. **125**, 030506 (2020).
[31] H. Zhu and M. Hayashi, Efficient Verification of Pure Quantum States in the Adversarial Scenario, Phys. Rev. Lett. **123**, 260504 (2019).
[32] Y.-C. Liu, J. Shang, R. Han, and X. Zhang, Universally Optimal Verification of Entangled States with Nondemolition Measurements, Phys. Rev. Lett. **126**, 090504 (2021).
[33] A. Dimić and B. Dakić, Single-copy entanglement detection, npj Quantum Inf. **4**, 11 (2018).
[34] V. Saggio, A. Dimić, C. Greganti, L. A. Rozema, P. Walther, and B. Dakić, Experimental few-copy multipartite entanglement detection, Nat. Phys. **15**, 935 (2019).
[35] J. M. Renes, R. Blume-Kohout, A. J. Scott, and C. M. Caves, Symmetric informationally complete quantum measurements, J. Math. Phys. (N.Y.) **45**, 2171 (2004).
[36] A. Roy and A. J. Scott, Weighted complex projective 2-designs from bases: Optimal state determination by orthogonal measurements, J. Math. Phys. (N.Y.) **48**, 072110 (2007).
[37] See Supplemental Material at http://link.aps.org/supplemental/10.1103/PhysRevLett.128.020502 for the theoretical and experimental details, which includes Refs. [38,39].
[38] Z. Hou, H. Zhu, G. Y. Xiang, C. F. Li, and G. C. Guo, Error-compensation measurements on polarization qubits, J. Opt. Soc. Am. B **33**, 1256 (2016).
[39] M. Ježek, J. Fiurášek, and Z. Hradil, Quantum inference of states and processes, Phys. Rev. A **68**, 012305 (2003).
[40] P. G. Kwiat, E. Waks, A. G. White, I. Appelbaum, and P. H. Eberhard, Ultrabright source of polarization-entangled photons, Phys. Rev. A **60**, R773 (1999).